Journal of Sol-Gel Science and Technology (2022) 102:208–218
https://doi.org/10.1007/s10971-021-05680-1

ORIGINAL PAPER: NANO-STRUCTURED MATERIALS (PARTICLES, FIBERS, COLLOIDS, COMPOSITES, ETC.)

Nanoencapsulation of isotropic and anisotropic particles through a green chemistry aerosol method: a scalable approach for ad-hoc surface tuning

Esteban A. Franceschini[1] · Gustavo Giménez[2] · M. Verónica Lombardo[3] · Andrés Zelcer[4,5] · Galo J.A.A. Soler-Illia[6,7]

Received: 20 May 2021 / Accepted: 28 October 2021 / Published online: 23 November 2021

Abstract

The interest in core–shell materials with chemically tunable mesoporous surfaces has significantly grown in recent years. The main limitation to obtain these systems through sequential precipitation is the tuning of the core and shell sol-gel chemistry, which usually implies low concentrations and leads to high-quality colloids although in small quantities after a lengthy and costly process. Aerosol approaches can lead to faster production and easier separation of functional materials with well-defined architectures. We present a "green chemistry" general method to coat sub-micron colloidal particles with a variety of mesoporous metal oxide nanofilms via an aerosol synthesis technique. Different types of particulate supports with isotropic and anisotropic shapes were dispersed into the precursor solutions in order to synthesize a mesoporous shell keeping the shape of the support. We chose the synthesis of TiO_2 and $TiSiO_4$ nanofilms on conventional Stöber SiO_2 spherical particles, and on anisotropic micronized mica particles as a case study. We used the commercial surfactant Pluronic® F127 as a porogen. The structure and composition of the obtained nanofilms were characterized by electron microscopy, X-ray diffraction, focused ion beam coupled to SEM, and nitrogen adsorption/desorption isotherms. The TiO_2 shells obtained (with an anatase-like structure) have pore diameters between 3.9–4.8 nm depending on the support with film thicknesses of ~100 nm, while amorphous $TiSiO_4$ shells have larger diameters (9.5–16 nm) with film thicknesses of between 50 and 200 nm depending on the support used. The method presented shows high reproducibility and, unlike batch methods, allows the continuous production and straightforward recovery of the materials.

Supplementary information The online version contains supplementary material available at https://doi.org/10.1007/s10971-021-05680-1.

✉ Esteban A. Franceschini
esteban.franceschini@mi.unc.edu.ar

✉ Galo J.A.A. Soler-Illia
gsoler-illia@unsam.edu.ar

[1] INFIQC-CONICET, Dto. de Fisicoquímica—Facultad de Ciencias Químicas, Universidad Nacional de Córdoba, Ciudad Universitaria, 5000 Córdoba, Argentina

[2] Departamento de Nanomateriales Funcionales, Dirección técnica de Micro y Nanoelectrónica, Instituto Nacional del Tecnología Industrial, Av. Gral Paz 5445 (B1620WAB) San Martín, Buenos Aires, Argentina

[3] Gerencia Química, Instituto de Nanociencia y Nanotecnología (INN-CONICET) Centro Atómico Constituyentes, Comisión Nacional de Energía Atómica, CONICET, Av. Gral Paz 1499 (B1650KNA) San Martín, Buenos Aires, Argentina

[4] CIBION, CONICET, Godoy Cruz 2390 (C1425FQD), CABA, Argentina

[5] ECyT-UNSAM, 25 de Mayo y Francia, C.P. 1650 San Martín, Buenos Aires, Argentina

[6] Instituto de Nanosistemas, Universidad Nacional de General San Martín, Av. 25 de Mayo 1021, 1650 San Martín, Argentina

[7] DQIAyQF, Fac. de Ciencias Exactas y Naturales, Universidad de Buenos Aires, Pabellón 2, Ciudad Universitaria, 1428 Buenos Aires, Argentina

Graphical Abstract

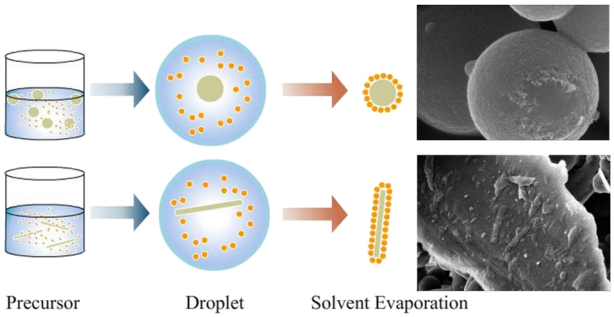

Keywords Mesoporous materials · Aerosol processing · Core–shell · Titania · Silica

Highlights

- An aerosol method for coating sub-micron particles with mesoporous metal oxide films is presented.
- Stöber SiO_2 spherical particles or anisotropic micronized mica particles were used as substrates.
- The use of aqueous solutions represents an eco-friendly approach to the synthesis of nanomaterials.
- This method is straightforward and permits the easy production of core-mesoporous shell nanoparticles.

1 Introduction

The rational design of nanomaterials is currently one of the main ways to prepare multifunctional core–shell nanocomposites, much needed for many emerging technological fields [1, 2]. To this end, the development of methods that allow surface modification of nanostructures in a simple, reproducible, and industrially scalable manner is of enormous interest [3].

The synthesis of core–shell materials having a mesoporous shell has generated much interest during the last years due to their potential uses [4–6] which derives from both, the intrinsical properties and wide range of mesoporous materials that can be synthesized [7]. Some of the most sought applications for mesoporous coatings include surface protection [8–10], molecular switching [11–13], energy applications [14–17], theranostics [18], etc.

Mesoporous nanofilms (shell) on spherical particles (core) have been presented in literature several times [19–22]. Sato and coworkers [23] presented a two-pot approach to synthesize double mesoporous core–shell silica spheres with a uniform size of 245–790 nm, shell thickness of 41–80 nm, and surface area and total pore volume of 141–618 $m^2\,g^{-1}$ and 0.14–0.585 $cm^3\,g^{-1}$, respectively. Solid silica spherical particles, used as the core, were synthesized by the Stöber method and a mesoporous shell could be formed around the silica cores by using an anionic surfactant and a co-structure directing agent. Liu et al. [24] synthesized core–shell Fe_3O_4@SiO_2 and core–shell–shell Fe_3O_4@nSiO_2@mSiO_2 with a mean diameter of around 300–400 nm and magnetic mesoporous silica Fe_3O_4@nSiO_2@mSiO_2 microspheres that can not only exhibit excellent adsorptive performance for removal of DDT (1,1,1-trichloro-2,2-bis(4-chlorophenyl) ethane) from aqueous media but also display high catalytic activity. Wen and coworkers [6] synthesized MnO_2@colloid carbon spheres nano-composites with tunable interior architecture and a diameter of around 500 nm.

More recently, Zhao and co-workers [25] synthesized mesoporous core–shell nanostructures using a confined interfacial monomicelle assembly method for the controlled coating of anatase TiO_2 with single-layered ordered mesopores on diverse surfaces. This method relies on the solvent-confinement effect of glycerol during the assembly process and monomicelle hydrogel preformation by selective evaporation of double-solvent precursors. Thus, the assembly process appears to be controllable for the synthesis of TiO_2 layers with highly tunable thickness.

The methods mentioned above, although of interest, are not general and can be used only to coat spherical supports and, usually, are developed to be applied to a single type of metal oxide. Furthermore, a much greater challenge is presented when trying to synthesize mesoporous nanofilms on anisotropic structures maintaining the original geometry of the support. It is important to consider that in many cases the correct integration between the core and the shell depends strongly on the physical and chemical interactions of the surface of the particle used as core, where the shell nucleates and grows, which also depends on the medium in which the supports are found and the synthesis conditions. In this context, aerosol methods present an enormous potential, due to the versatility of the processing and to the independent control of the hydrolysis and condensation

processes in the initial solutions, plus the high control of the self-assembly processes along with droplet drying [26–28]. This synthetic method has been explored in the last decade, either from molecular or from nanocrystalline pre-formed building blocks [29]. Nowadays, the "aerosol-assisted sol-gel" process allows, for example, the preparation of a large variety of highly active heterogeneous catalysts. [30]. Among the huge possibilities, the inclusion of colloidal objects in the starting sols permits the development of core–shell systems that can also be turned into hierarchically porous materials [29].

In a previous work [31], we presented a general method for the synthesis of a variety of mesoporous MO_2 spherical particles (M = Ti, Zr, Ce, and their mixed oxides) that allows the continuous production of these materials in large quantities of submicron-scale mesoporous oxides with a yield over 95%. Moreover, the use of aqueous solutions allows working in an air atmosphere, where organic solvents could ignite or explode, making this method much safer, cheaper, and more environmentally friendly than those based on the use of concentrated hydrochloric acid and organic solvents.

In this work, we present a method for the synthesis of core–shell structures by coating pre-formed cores with mesoporous nanofilms. We show the versatility of the method using two different types of supports (cores), and two types of nanofilms (shells) synthesized on each support. The selected supports vary in their morphology and chemistry, being either isotropic silica colloids as well as anisotropic micronized mica platelets, proving that the method is suitable for different support shapes. Mica particles are inexpensive and widely used in industrial applications in paints, plastics, adhesives, lubricants, rubbers modifications, disinfectants, etc., and the possibility of tuning its surface properties adds value to a commodity material.

Furthermore, the process used in this paper is based on a general method that allows the synthesis of various mesoporous metal oxide (and mixed metal oxides) nanomaterials virtually without changing the formulation of the precursor mixture. In this work, we adapted that method for the synthesis of nanofilms on a variety of substrates with different geometries. This allows us to foresee the possibility of synthesizing other mesoporous oxides using the same method. Additionally, unlike controlled precipitation methods, where the mass of synthesized materials is low and normally requires a long synthesis time, this method is suited for continuous production of the materials with minimum requirements of reactivity control. This is a fundamental feature required for the industrial application of core–shell materials. While in batch solution methods the surface–sol interaction plays a central role since it determines whether a shell will be formed or the nucleation of new particles will take place, in this method its role is not so preponderant. Thanks to the fast sol evaporation during the process, as long as the sol wets the support with a low contact angle a shell will be formed. Therefore, we envisage that it should be possible to apply this method for other combinations of support and shell as long as the sol wets the support surface. This method could be easily used to synthesize a wide range of materials with optical, catalytic, and photochemical properties, make ceramic coatings, give or improve ion trapping properties, etc., depending on the type of support and/or coating used.

2 Experimental

2.1 Materials

Triblock poly(ethylene oxide)-b–poly(propylene oxide)-b–poly(ethylene oxide) copolymer $EO_{106}PO_{70}EO_{106}$, denoted Pluronic® F127 (Mw = 12.600, Aldrich), Titanium(IV) isopropoxide 97% (Aldrich), Glacial acetic acid (Merck), acetylacetonate (Merck) tetraethoxysilane (98%, TEOS, Aldrich), Na_2SiO_3 (SiO_2, 50–53%, Aldrich), absolute ethanol (99.8%, Merck), ammonium hydroxide (Merck) were used as received. Micronized mica was kindly provided by Lanxess Argentina. All aqueous solutions were prepared with deionized water having resistivity ≈18.2 MΩ cm^{-1}, and degassed using high purity N_2 (Indura S.A.).

2.2 Synthesis

Mesoporous metal oxide nanofilms precursors solutions were prepared from stabilized metal precursor solutions containing a suspension of the core particles. First, a complexing mixture was prepared by mixing 2.775 g of glacial acetic acid with an equivalent mass of acetylacetonate. Then, 1.2×10^{-3} mol of the titanium (IV) isopropoxide was added. This mixture was stirred for 15 min and subsequently, either 72.5 g of Milli Q water, for the TiO_2 precursor solutions, or a mixture of 15 mL of 0.1 M Na_2SiO_3 solution and 57.5 mL of Milli Q water, for the $TiSiO_4$ precursor solutions, were added dropwise. Then, 0.2 g of Pluronic® F127 was added as template agent and the final solution was kept under stirring until complete dissolution. Finally, 10 mL of the dispersed supports (see concentrations below) were added to the metal oxide precursor solutions.

Silica supports were synthesized employing the Stöber method [32] using the appropriated amounts of absolute ethanol, ammonium hydroxide, and Milli Q water to obtain particles with ~500 nm in diameter [32].

The support suspensions (either silica colloids or micronized mica) were prepared by dispersing 0.5 g of the material in 40 mL of Milli Q water and sonicating for 15 min.

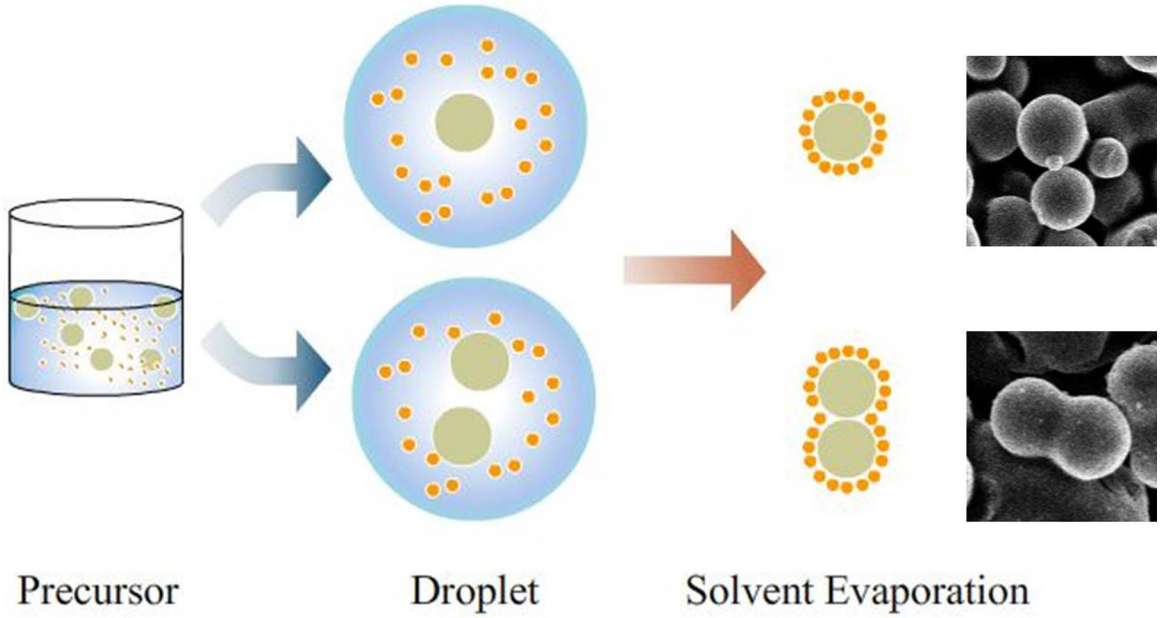

Fig. 1 Aerosol nanofilm synthesis scheme

The synthesis dispersion was aerosolized using a Mini Spray Dryer Büchi B-290 using as carrier gas N_2, an inlet temperature of 220 °C, and a flow rate of 44 $m^3 h^{-1}$ [31]. After obtaining the aerosol all samples were calcined at 350 °C for 2 h with a heating rate of 1 °C min^{-1}. Figure 1 shows a schematic representation of the nanofilms synthesis. In a single run, we prepared up to 2 g of coated particles using this laboratory-sized equipment.

3 Structural characterization

Field Emission Scanning Electron images were obtained using a Supra 40 (Zeiss Company) FESEM operating at a voltage of 3 kV, equipped with an Oxford EDS and backscattering detector.

Nitrogen adsorption–desorption isotherms of samples were measured at 77 K on a Micromeritics ASAP 2420 NSP instrument after outgassing samples at 150 °C. The surface area was calculated by using the Brunauer–Emmett–Teller equation. Total pore volume was obtained at $P/P_0 = 0.98$. Pore size was obtained from the desorption branch using the BJH model [33].

In order to measure the thickness and analyze the interphase of the different core–shell structures, a cross-section analysis was performed using a Helios NanoLab 650 (FEI) focused ion beam-scanning electron microscopy. A localized Pt thin film (150 nm) was deposited on the sample to protect it, and a gallium ion column was used to prepare a lamella of the portion of interest.

Transmission Electron Microscope (TEM) images were acquired with a Philips EM 301.

X-ray diffractograms were obtained using the Cu Kα radiation ($\lambda = 1.5406$ Å), using a PANalytical X'Pert PRO diffractometer (40 kV, 40 mA), with the θ–2θ Bragg–Brentano geometry. The 2θ range used was from 10° to 70°, with steps of 0.02° and a counting time of 1 s per step. The FULLPROF program [34] was employed to refine the crystal structure by the Rietveld method. The data refined were lattice parameters, peak shape, atomic positions, isotropic thermal parameters, and occupation factors.

4 Results and discussion

4.1 Electron microscopy analysis

Four different types of samples were prepared, combining the two types of supports and two types of mesoporous nanofilms. The supports consisted of colloidal silica spheres with a diameter of ca. 500 nm, and highly anisotropic micronized mica platelets. The mesoporous nanofilms materials were either TiO_2 or $TiSiO_4$. In order to simplify the notation, the samples are labeled indicating the shell material followed by the support material, so TiO_2 mesoporous shells over SiO_2 particles are denoted as Ti/Si, while $TiSiO_4$ shells over the same support are denoted as TiSi/Si. In the same way, TiO_2 nanofilms shells on mica supports are denoted as Ti/Mi and mesoporous $TiSiO_4$ nanofilms on mica as TiSi/Mi.

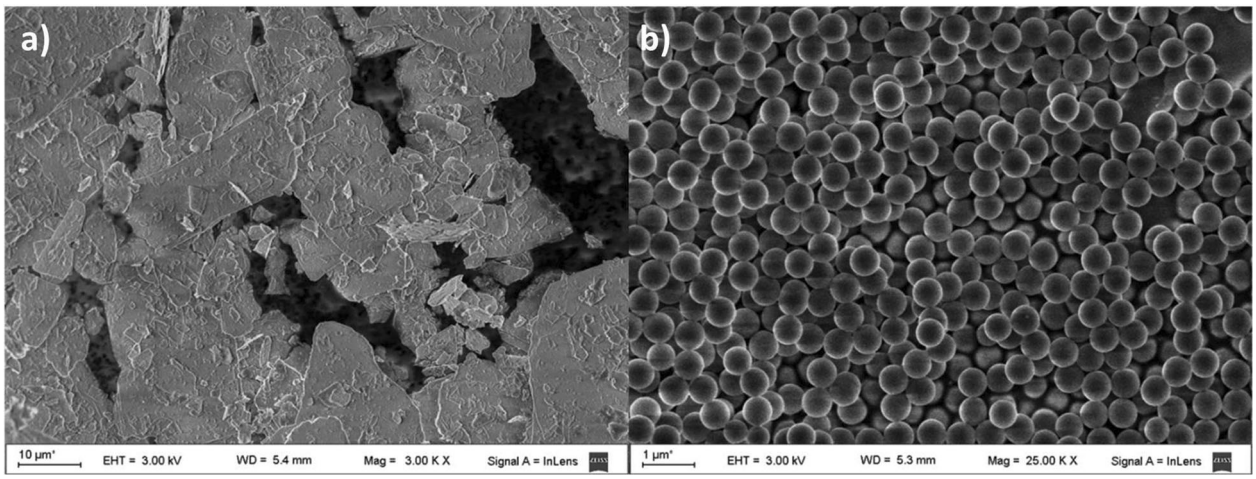

Fig. 2 SEM images of supports. **a** Micronized mica plates, **b** silica colloids

Figure 2 shows SEM images of both supports used, micronized mica (Fig. 2a) and silica colloids (Fig. 2b) supports before the nanofilms synthesis. The micronized mica presents an anisotropic laminar shape with an area of some tens of square microns and a thickness of a few tens of nanometers. Silica colloids, on the contrary, have an isotropic shape and a highly monodisperse size distribution, as is expected for particles obtained using the Stöber method. In the next section, the results of the different films synthesized on these supports are presented.

4.1.1 Mesoporous TiO_2 nanoshell

Figure 3 shows SEM images with different magnifications of the samples Ti/Mi (a and b) and Ti/Si (c and d). The core–shell particles maintained the original morphology of the supports, even when coated by the mesoporous TiO_2 film. The pore diameter is about 8 nm, which is common for materials obtained using Pluronic® F127 [35–38].

The images show the presence of agglomerates covered by a nanofilm layer, which encloses usually one, but sometimes two or more support particles (it is easier to see in the Ti/Si sample). These are possible due to the presence of more than one support particle per aerosol drop (Fig. 1). The balance between surface tension and hydrodynamic forces in the nozzle exit determines the initial size of the aerosol droplet. Despite the presence of surfactant, the formation of smaller droplets is inhibited as most of the liquid remains attached to the surface of the particles by surface tension.

Big agglomerates of support nanoparticles are not observed. This indicates that the support particles form a stable dispersion in the precursor solution. The use of water as a solvent is a key feature of this method since its high dielectric constant together with the presence of a surfactant agent stabilizes the colloidal particles, even in the presence of metal precursors and acid conditions.

The particle size distribution of the Ti/Si sample and the SiO_2 support, which have spherical geometry, were obtained from SEM images. At least 150 particles of each sample were measured, excluding agglomerates from the analysis (Fig. S1, see supporting information). An increase in the average particle size of ~150 nm compared to the original size is noted, which means that the particles are coated by a nanofilm of about 75 nm.

The EDS analysis confirms the addition of Ti to the matrix components of both supports and discards the presence of metallic impurities.

TEM images of the Ti/Mi and Ti/Si samples are shown in Fig. 4a, b, respectively. Although TEM penetration is not high enough to completely cross the central part of the samples, the porosity is clearly observed in the edges of the particles. The mesoporous layers present a different thickness depending on the type of support used. The film thickness in the Ti/Si sample is about 100 nm, while for the Ti/Mi sample thickness is slightly higher.

Cross-section cuttings of the samples were performed by focused ion beam (FIB), in order to better study the thickness of the nanofilms over the different supports. Figure 5 shows scanning electron images of cross-sections obtained for both mesoporous TiO_2 coated samples: Ti/Si and Ti/Mi. Figure 5a shows the cross-sectional profile obtained by scanning electron microscopy of a coated micronized mica plaque. A uniform layer of mesoporous TiO_2 nanofilm of about 200 nm thickness is visible on both sides. Figure 5b shows an SEM image of the cross-section of the Ti/Si sample, in which the silica colloid support is coated by a uniform mesoporous nanofilm layer, about 80 nm in thickness. This thickness is consistent with the average obtained

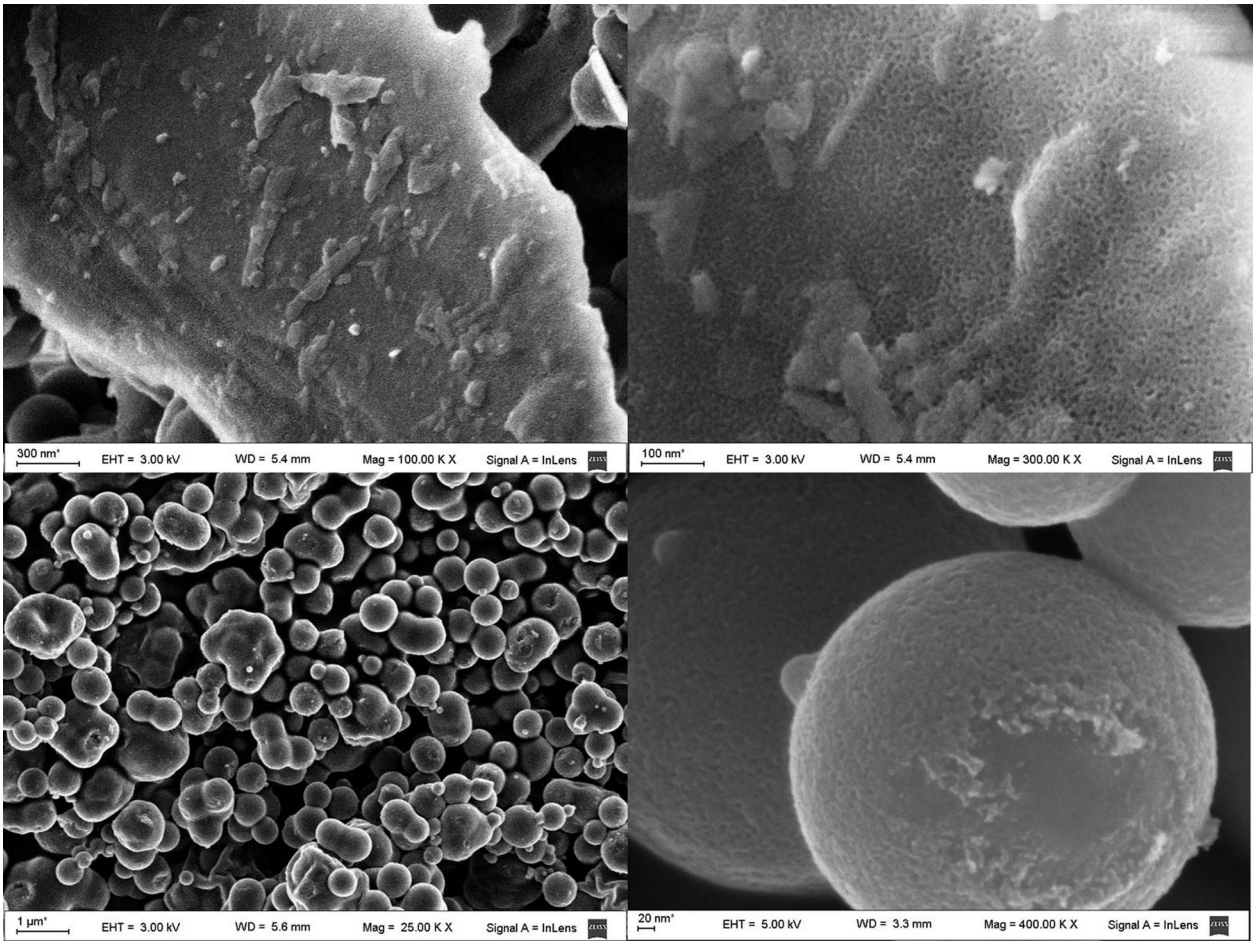

Fig. 3 SEM images of **a**, **b** Ti/Mi and **c**, **d** Ti/Si nanofilms

through the analysis of the transmission electron microscopy images.

4.1.2 Mesoporous $TiSiO_4$ nanoshell

Figure 6 shows scanning electron micrographies with different magnifications of the samples TiSi/Mi (a and b) and TiSi/Si (c and d). As for TiO_2 nanofilm coated samples, $TiSiO_4$ samples maintain the original morphology of the supports.

The presence of agglomerates is most noticeable in the TiSi/Si sample than in the case of Ti/Si. Histograms of the particle size distribution of the TiSi/Si sample (Fig. S1) were compared with the histograms obtained for the silica support before the nanofilm formation and the Ti/Si sample. An increase in the average particle size of ~250 nm in comparison with the original size of the support is observed, and about 100 nm greater than Ti/Si particles. This increase in diameter would indicate the presence of a ~150 nm thick nanofilm. This larger thickness is due to the amount of oxide precursor in the aerosol dispersion, which contains not only the Ti precursor but also the sodium silicate. Moreover, the higher concentration leads to increased viscosity and changes the surface tension of the suspension. This leads to differences in droplet formation and evaporation dynamics. From the SEM images, it is possible to determine the percentage of core-less particles for the Ti/Si systems, being about 13.7% of the total synthesized particles, 74% are core–shell particles with a single core, 6.6% are agglomerates of two cores wrapped in a single shell and 5.7% are particles with three or more cores so that most of the synthesized particles have a defined core–shell structure.

The EDS analysis confirms the addition of Ti and Si to the matrix components of both supports and discards the presence of metallic impurities.

In Fig. 4c, d, TEM images of the TiSi/Si and TiSi/Mi samples are shown respectively. In these cases, the presence of Si in the oxide matrix permits a higher penetration of the electron beam in the sample. The mesoporous layers show a homogeneous thickness that, as above, depends on the type of support used.

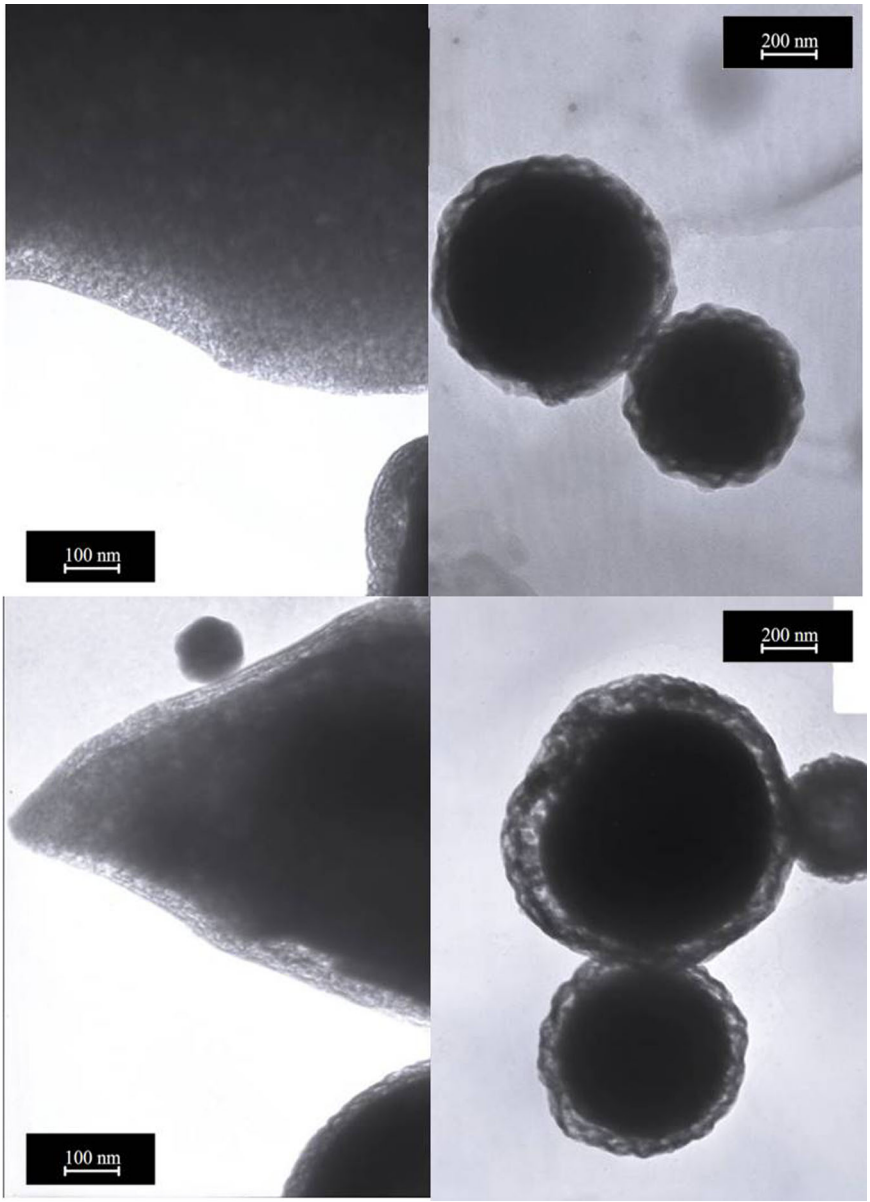

Fig. 4 TEM images of **a**, **b** Ti/Mi and **c**, **d** Ti/Si nanofilms

Cross-sectional analysis carried out in the TiSi/Si and TiSi/Mi samples (Fig. 5c, d, respectively) shows that the micronized mica plaque is coated on both sides by a uniform $TiSiO_4$ mesoporous nanofilm of about 200 nm in thickness while the Si spheres show a uniform film of about 50 nm. The differences found between the two supports are probably due to the fact that although the mass used of both supports was the same, their surface areas are very different, and SiO_2 particles are expected to have a higher surface area per gram than micronized mica.

4.2 Nitrogen adsorption

All isotherms obtained are type IV, characteristics of mesoporous materials [39]. In the case of samples Ti/Si and Ti/Mi, Point B, which corresponds to the complete formation of monolayer and the beginning of multilayer adsorption, can be seen very well defined in Fig. 7a. In the cases of TiSi/Si and TiSi/Mi, it is not shown so clearly because this occurs with a low amount of N_2 adsorbed. This corresponds to the lower surface areas that both samples present (Table 1). The hysteresis cycle is a clear H3 type [40], for the TiSi/Si, TiSi/Mi, and Ti/Si samples. This type of hysteresis is characteristic of materials with a wide pore size distribution, and the pores are slit type. For the Ti/Mi sample, the hysteresis cycle is more similar to an H2 cycle, which is a bit difficult to interpret. We propose that this feature is due to "bottleneck" type pores or percolation effects due to the interconnection in the pore network [41]. In these cases, the pore distribution is narrower.

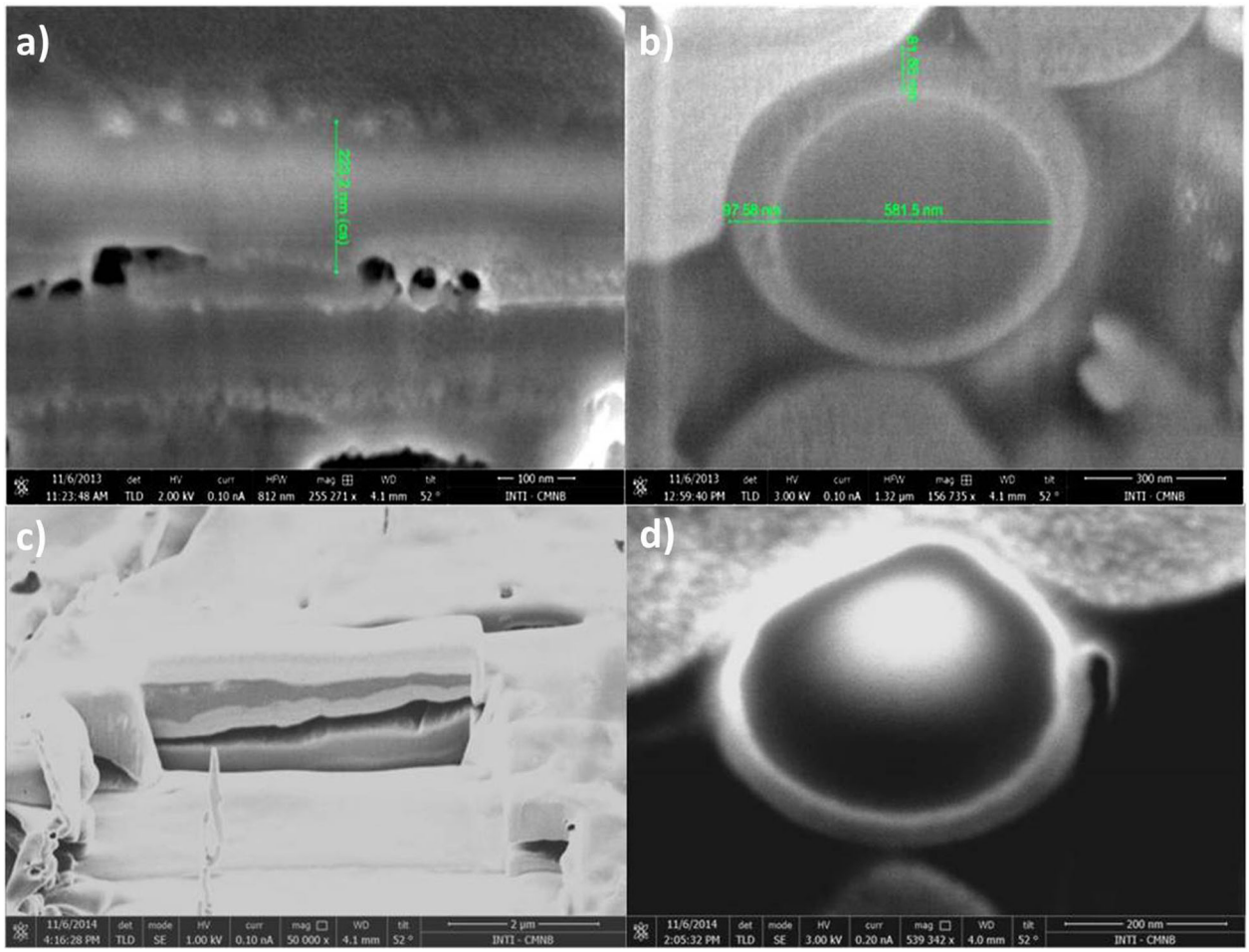

Fig. 5 SEM images of the side view of **a**, **c** Ti/Mi and **b**, **d** Ti/Si nanofilms cut with Focussed Ion Beam

For Ti/Si sample, pore size distribution has a maximum at 4.8 nm, but there are pores with diameters between 2 and 14 nm with a major proportion of bigger pores. When the support is micronized mica (Ti/Mi) pore size distribution is narrower, with a maximum at 3.9 nm (Fig. 7b). When the shell is $TiSiO_4$, we observed wider distribution of pores than when the shell is only formed by TiO_2.

A study of the profile plots took from the transmission electron micrographies was carried out, where the porosity is more evident (Fig. S2), which allowed estimating an interpore distance of 9.0, 7.2, 18.6, and 19.0 nm for Ti/Si, Ti/Mi, TiSi/Si, and TiSi/Mi, respectively. From these data and the pore size obtained by N_2 sorption, we can estimate a wall thickness: Ti/Si 4.2 nm, Ti/Mi 3.3 nm, TiSi/Si 9.1 nm, and TiSi/Mi 3.0 nm. It can be inferred that the system with a smaller pore size brings with it a lower wall thickness of TiO_2, with the exception of the TiSi/Mi sample. In this case, in addition to the fact that the micrograph is not very adequate to carry out this analysis, the pore size distribution obtained by the N_2 isotherm is very wide, therefore, the wall thickness cannot be estimated under these conditions.

4.3 X-ray diffraction analysis

X-ray diffractograms were measured for the two supports used and the different materials synthesized on each support. Figure 8a, b shows the different diffractograms obtained. It can be seen that the mica has a well-defined crystalline structure, with characteristic peaks that are also found in the TiO_2 and TiO_2-SiO_2 coated samples. As expected, the SiO_2 particles are amorphous and do not show any characteristic peaks in the diffractogram [42, 43].

Regardless of the support used, no peaks corresponding to TiO_2-SiO_2 are observed, indicating that this compound has an amorphous structure as expected [44–46]. On the contrary, TiO_2 nanofilms in both supports present a peak at 25.4° corresponding to TiO_2 with an anatase-like structure [47] with low amorphousness with a full width at half maximum of ~1.6° indicating a crystallite size of ~5 nm regardless of the support used. This crystallization is consistent with

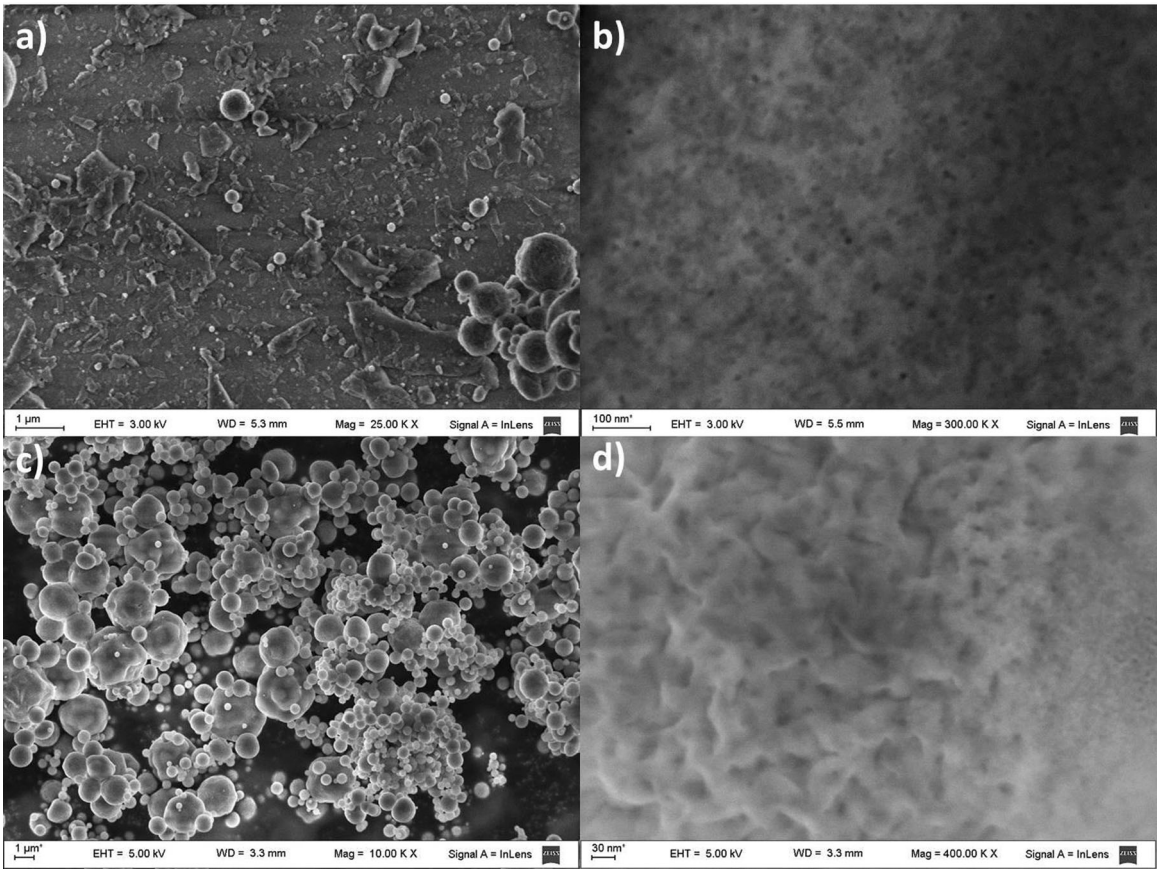

Fig. 6 SEM images of **a**, **b** TiSi/Mi and **c**, **d** TiSi/Si nanofilms

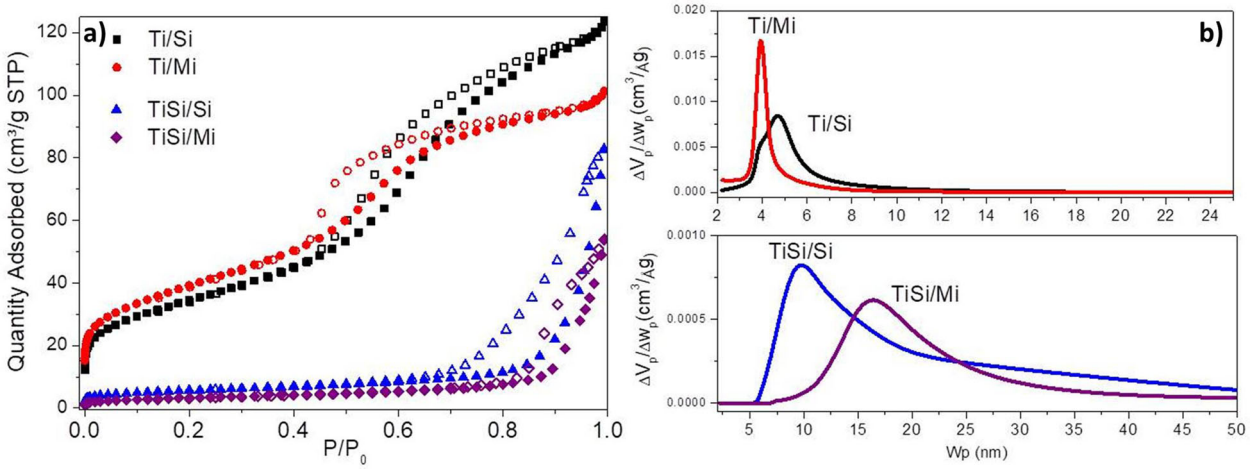

Fig. 7 **a** Nitrogen adsorption (closed)–desorption (open) curves for Ti/Si (■), Ti/Mi (●), TiSi/Si (▲), and TiSi/Mi (♦). **b** Pore size distributions obtained from the desorption branch of the nitrogen isotherms

previous work in both aerosols [48] and films on silicon or silica-coated glass or ITO substrates [49, 50].

Figure 8b shows at 28.5° a peak corresponding to the silicon support on which the Ti/Si and TiSi/Si core–shell powder samples were deposited on measuring [51].

5 Conclusions

In this work, we present a simple method for the synthesis of mesoporous nanoshells in the aerosol phase over substrates with different morphologies. The method used

is water-based and allows the preparation of a variety of mesoporous materials. The nanofilms synthesized completely cover the surface of the used substrate, even when anisotropic structured support is employed; generating a mesoporous layer that reproduces the structure of the support.

Table 1 Surface and pores features of samples

	Surface area (m^2/g)	Mesopore volume cm^3/g	Pore diameter (nm)
Ti/Si	124	0.19	4.8
Ti/Mi	141	0.12	3.9
TiSi/Si	20	0.10	9.5
TiSi/Mi	12	0.07	16.0

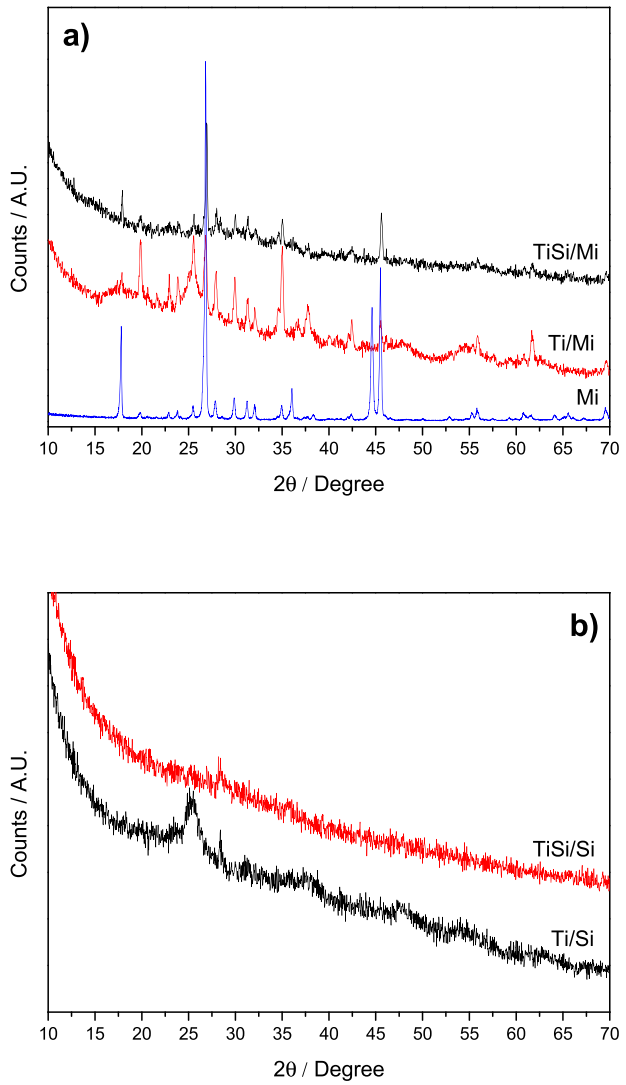

Fig. 8 X-ray diffraction pattern of the film-coated supports, **a** micronized mica and, **b** SiO_2 colloid supports

The uniform covering of anisotropic structures, as is the case of the micronized mica support, is obtained due to the short retention time to which the samples are subjected during the aerosol formation process, and is very difficult to achieve by conventional chemical means, which usually yield spherical core–shell particles. Moreover, we successfully prepared 2 g of Ti/Si particles in one run, using a laboratory-sized mini spray dryer, using a fraction of solvent volume and synthesis times much shorter compared to batch methods.

A clear incidence of the substrate used to synthesize the nanofilm was observed by N_2 sorption, as well as the composition of the oxide in the material type obtained. When the film is made by a simple oxide, we obtained greater surface areas and smaller pore diameters, although accompanied with a narrow size distribution than in the case of a mixed oxide. This distribution of sizes is narrower when the substrates are micronized mica than when the support is SiO_2 nanoparticles.

The aerosol-assisted sol-gel method used in this work for the synthesis of mesoporous shells allows to easily generate mesoporous structures with a variety of chemical compositions. This method could be adapted for the synthesis of mesoporous shells on the surface of materials with well-defined morphology commonly used on a laboratory scale (such as silica colloids), as well as materials with ill-defined shapes usually encountered in nature and used on an industrial scale (as micronized mica). The surface customization and tuning of commonly used fillers and supports were carried out by a simple and environmentally friendly method, adding value and extending the range of applications of these materials.

Acknowledgements The authors thank financial support from Agencia Nacional de Promoción Científica y Tecnológica (PICT 2015-3625, PICT 2015-3853, PICT Start Up 2017–4651, PICT 2017-0250, PUE2017-INFIQC, FSNANO 2010-007, PICT 2018-04236) and CONICET. We gratefully acknowledge M.C. Marchi (CMA, FCEN, UBA) for the SEM images and N. de Vicenzo for the TEM. GG is researcher in the FIB Microscopy Lab (INTI). MVL, AZ, EAF, and GJAAS-I are permanent research fellows of CONICET.

Author contributions Conceptualization: [Esteban Franceschini] [Galo Soler Illia]; Methodology: [Galo Soler Illia], [Andres Zelcer]; Formal analysis and investigation: [Esteban Franceschini] [M. Veronica Lombardo] [Gustavo Gimenez]; Data Analysis: [All authors]; Writing—original draft preparation: [Esteban Franceschini] [M. Veronica Lombardo]; Writing—review and editing: [All Authors]; Funding acquisition: [Galo Soler Illia] [Esteban Franceschini]; Resources: [Galo Soler Illia] [Esteban Franceschini]; Supervision: [Galo Soler Illia].

Funding ANPCYT PICT 2015-3625, ANPCYT PICT 2015-3853, ANPCYT PICT Start Up 2017–4651, ANPCYT PICT 2017-0250, CONICET PUE2017-INFIQC, FSNANO 2010-007.

Compliance with ethical standards

Conflict of interest The authors declare no competing interests.

Publisher's note Springer Nature remains neutral with regard to jurisdictional claims in published maps and institutional affiliations.

References

1. Shen X, Zheng Q, Kim JK (2021) Prog. Mater. Sci. 115:100708
2. Kim MS, Kim JW, Yun J et al. (2020) Appl. Surf. Sci. 515:146018
3. Spoljaric S, Ju Y, Caruso F (2021) Chem. Mater. 33:1099
4. Deng Y, Qi D, Deng C et al. (2008) J. Am. Chem. Soc. 130:28
5. Yang Y, Guo X, Wei K et al. (2014) J. Nanoparticle Res. 16:2210
6. Zhang Y, Dong M, Zhu S et al. (2014) Mater. Res. Bull. 49:448
7. Ren, Y Ma, Z Bruce PG (2012) Chem. Soc. Rev. 41:4909
8. Ouyang Y, Li L-X, Xie Z-H et al. (2020) J. Magnes. Alloy. 15
9. Xiong L, Liu J, Li Y et al. (2019) Prog. Org. Coatings 135:228
10. Castaldo R, de Luna MS, Siviello C et al. (2020) J. Cult. Herit. 44:317
11. Zhang Z, Runa A, Wu J et al. (2019) Chinese Chem. Lett. 30:779
12. Saadaoui M, Fernández I, Sánchez A et al. (2015) Electrochem. Commun. 58:57
13. Luo W, Xu X, Zhou B et al. (2019) Mater. Sci. Eng. C 100:85
14. Bruno MM, Franceschini EA, Planes GA et al. (2009) J. Appl. Electrochem. 40:257
15. Franceschini EA, Gomez MJ, Lacconi GI (2019) J. Energy Chem. 29:79
16. Jiang J, Kucernak A (2002) J. Electroanal. Chem. 520:64
17. Gautam J, Thanh TD, Maiti K et al. (2018) Carbon N. Y. 137:358
18. Lee JE, Lee N, Kim T et al. (2011) Acc. Chem. Res. 44:893
19. Li Z, Liu M, Fan L et al. (2014) Biosens. Bioelectron. 52:293
20. Ling Y, Long M, Hu P et al. (2014) J. Hazard. Mater. 264:195
21. Lv Q, Li G, Sun H et al. (2014) Microporous Mesoporous Mater. 186:7
22. Sun Y, Sun Y, Wang L et al. (2014) Microporous Mesoporous Mater. 185:245
23. Mohamed El-Toni A, Khan A, Abbas Ibrahim M et al. (2012) J. Colloid Interface Sci. 378:83
24. Liu F, Tian H, He J (2014) J. Colloid Interface Sci. 419:68
25. Lan K, Xia Y, Wang R et al. (2019) Matter 1:527
26. Faustini M, Boissière C, Nicole L et al. (2014) Chem. Mater. 26:709
27. Boissiere C, Grosso D, Chaumonnot A et al. (2011) Adv. Mater. 23:599
28. Franceschini EA, *Nanostructured Multifunctional Materials Synthesis, Characterization, Applications and Computational Simulation* (CRC Press, First Edition. | Boca Raton: CRC Press, Taylor & Francis, 2021)
29. Grosso D, Soler-Illia GJ de AA, Crepaldi EL et al. (2003) Adv. Funct. Mater. 13:37
30. Debecker DP, Le Bras S, Boissière C et al. (2018) Chem. Soc. Rev. 47:4112
31. Zelcer A, Franceschini EA, Lombardo MV et al. (2020) J. Sol-Gel Sci. Technol. 94:195
32. Stöber W, Fink A, Bohn E (1968) J. Colloid Interface Sci. 26:62
33. Thommes M (2010) Chemie-Ingenieur-Technik 82:1059
34. Rodríguez-Carvajal J (1993) Phys. B Phys. Condens. Matter 192:55
35. Alexandridis P, Hatton TA (1995) Colloids Surfaces A 96:1
36. Franceschini EA, Bruno MM, Viva FA et al. (2012) Electrochim. Acta 71:173
37. Franceschini EA, Planes GA, Williams FJ et al. (2011) J. Power Sources 196:1723
38. Velasco MI, Franzoni MB, Franceschini EA et al. (2017) J. Phys. Chem. C 121:7533
39. Rouquerol F, Rouquerol J, Sing K (1999) Vak. Forsch. Und Prax. 11:191
40. Gregg SJ, Sing K, *Adsorption, Surface Area, and Porosity*, Second (Academic Press, London, 1982)
41. Thommes M, Kaneko K, Neimark AV et al. (2015) Pure Appl. Chem. 87:1051
42. Dhanalekshmi KI, Sangeetha K, Meena KS et al. (2019) Photodiagnosis Photodyn. Ther. 26:79
43. Bai A, Song H, He G et al. (2016) Ceram. Int. 42:7583
44. Cai T, Wang Y, Dong Y et al. (2013) Mater. Lett. 111:173
45. Sakthisabarimoorthi A, Britto Dhas SAM, Jose M (2020) Mater. Chem. Phys. 240:122154
46. Angelomé PC, Andrini L, Fuertes MC et al. (2010) 13:256
47. Yin JB, Zhao XP (2002) Chem. Mater. 14:4633
48. Araujo PZ, Luca V, Bozzano PB et al. (2010) ACS Appl. Mater. Interfaces 2:1663
49. Violi IL, Perez MD, Fuertes MC et al. (2012) ACS Appl. Mater. Interfaces 4:4320
50. Angelomé PC, Andrini L, Calvo ME et al. (2007) J. Phys. Chem. C 111:10886
51. Swanson HE, Fuyat RK, Ugrinic GM (1953) *Standard X-Ray Diffraction Powder Patterns*